AIAA

AIAA 2000-0536

Nonlinear Interaction of Görtler and Second Shear Modes in Hypersonic Boundary Layers

Chong W. Whang and Xiaolin Zhong
University of California, Los Angeles
Los Angeles, CA

38th Aerospace Sciences Meeting & Exhibit
January 10–13, 2000 / Reno, NV

Nonlinear Interaction of Görtler and Second Shear Modes in Hypersonic Boundary Layers

Chong W. Whang *and Xiaolin Zhong [†]

University of California, Los Angeles, California 90095

Abstract

Nonlinear development of Görtler vortices and interaction with second shear mode are considered in this paper. The nonlinear development distorts the mean flow and leads highly inflectional profiles not only in wall normal direction but also in spanwise direction which induce the secondary instability. In boundary layer flow along the concave surface, shear modes as well as Görtler modes exist when Reynold's number is large enough, and their interactions play an important role in transition of the flow along the concave surface. In this paper, nonlinear development of Görtler vortices and their effects on the relatively small amplitude of two dimensional second shear mode are investigated using Direct Numerical Simulation (DNS). Initial forcing disturbances are obtained from the Linear Stability Theory (LST), and subsequent linear and nonlinear development and its interaction with other modes are simulated using Navier-Stokes equations. We investigate nonlinear effects of Görtler vortices in hypersonic boundary layers.

1 INTRODUCTION

The transition of laminar/turbulent boundary layer flow is the fundamental subject in fluid mechanics. In general, boundary layer flows become turbulent in three steps: 1) receptivity, 2) linear growth of disturbance, and 3) nonlinear effects in which the flow breaks down to turbulence. Görtler instability is one of many B-L instability mechanisms. Görtler vortices appear in boundary layer flow along concave surfaces due to the imbalance between pressure and centrifugal force. Many practical engineering designs involve concave surfaces such as engine inlet. Therefore, Görtler instability becomes an important subject in fluid mechanics.

*Graduate Student, chong@seas.ucla.edu

[†]Associate Professor, Mechanical and Aerospace Engineering Department, Senior Member AIAA

Görtler vortices have been studied experimentally and numerically since Görtler found them in 1940 [1-29]. Liepmann [2] conducted boundary-layer transition experiments on concave walls and showed that the critical Reynold's number for concave walls is lower than for flat plates which means concavity destabilizes flow. Even though the Görtler instability has been theoretically estabilished since 1940, actual observation of Görtler vortices were conducted by Tani [3] in 1962. Using smoke, he observed a spanwise variations by velocity measurements along the concave wall.

Görtler instability has been studied using LST. Görtler [1] and Smith [4] showed neutral stability curves in their linear stability analysis. However, their results were not consistent to each other. They were only matched in the limit of the short wavelength, and Hall [5] [6] [7] applied asymptotic theory to Görtler instability problems. Hall [5] proved that in high wavenumber limit, the parallel flow theory becomes valid. Hall [7] obtained that the existence of a neutral point strongly depends on location and shape of the initial condition. However, Hall and Fu [8] in their asymptotic analysis showed that at hypersonic speed limit, the nonuniqueness of the neutral stability curve associated with incompressible Görtler vortices disappears.

El-Hady and Verma [9] computed complete stability digrams for various Mach number. Normal velocity and streamwise variations were included in their analysis. They proved compressibility is a stabilizing factor. Spall and Malik [10] dealt with linear stability theory of Görtler instability using method of marching in which streamwise variations of disturbances were also considered. In mean flow calculation, pressure changes in streamwise direction were included to study adverse pressure effects. Mach number range is 0-12 so they considered hypersonic as well as supersonic boundary layers. It was found that in hypersonic limit, compressibility effects become less important, and adverse pressure is a dominant role in flow instability.

Aihara [11] in his wind tunnel experiment showed that the non-linear development of Görtler vortices mainly affects the transition of the boundary lay-

ers. Sabzvari and Crane [12] and Peerhossaini and Wesfreid [13] observed mushroom like vortices due to the nonlinear growth of Görtler vortices. They showed there are two regions (upwash and downwash) in development of Görtler vortices. Peerhossaini and Wesfreid [13] observed interaction between two neighboring vortices.

Recent experiments have shown that breakdown of Görtler vortices is mainly due to secondary instabilities. Aihara and Kohama [14] and Aihara et al [15] identified the breakdown of the vortex structure as a secondary instability due to a horsesho-vortex structure. Swearingen and Blackwelder [16] verified two kinds of secondary instabilities which are the sinous and varicose types. They showed that sinuous mode is produced by spanwise velocity gradient, and the varicose is due to normal velocity gradient. In their experiments, the unsteady secondary instability fluctuations correlated better with the spanwise velocity than with the normal velocity gradient.

Recently many researchers have tried to solve nonlinear Görtler problems numerically. Hall [17] demonstrated that nonlinear evolution of streamwise Görtler vortices produces inflectional profiles which will presumably break down. Lee and Liu [18] and Liu [19] numerically showed mushroom like vortex due to nonlinear growth of Görtler vortices.

Liu and Domaradzki [20], Yu and Liu [21], and Li and Malik [22] studied secondary instability effects on Görtler vortices. Li and Domaradzki [20] dealt with Görtler problem using DNS. Initial disturbances were obtained from LST. They showed that Görtler vortices become turbulent due to the spanwise velocity gradient as well as the normal velocity gradient. These velocity profiles contain inflectional points which play roles in flow instability. They mentioned that varicose mode is related to the normal velocity gradient, and sinuous mode is to the spanwise gradient and concluded that sinuous mode is dominant. Li and Malik [22] used PSE (parabolic stability equation) method, and studied nonlinear effects of Görtler vortices. In their approach, they showed there are two kinds of secondary instability modes; even and odd. The even mode is related to the varicos mode, and the odd mode is to the sinous mode.

Nayfeh [23], in his multiple-scale analysis for two dimensional boundary layers, showed that Görtler vortices can interact with the oblique Tollmien-Schlichting (TS) waves whose spanwise wavelength is the twice of the vortices. He found that Görtler vortices strongly destablize the TS waves. Malik [24] obtained the results which are not agreed with Nayfeh. He found the incon-

sistent length scale in Nayfeh's formula and showed in his temporal and parallel analysis that the oblique TS waves whose wavelength is the half of the vortices are destabilized by the nonlinear interaction. Nayfeh and Al-Maaitah corrected [25] the formula and presented the new results which are the same to Malik [24]. They used both Floquet theory and the method of multiple-scale and showed both methods give a good agreement.

Malik and Hussaini [26] considered nonlinear interaction between two dimensional TS waves and Görtler vortices. In the analysis, incompressible Navier-Stokes equations are solved using a Fourier-Chebyshev spectral method. It is shown that the TS waves can be excited by Görtler vortices, and due to the nonlinear effects, Görtler vortices induces the oblique wave whose wavelength is the equal to the vortices.

2   Governing Equations

The unsteady three dimensional Navier-Stokes equations in conservative-law form are used for the direct numerical simulation:

$$\frac{\partial U^*}{\partial t^*} + \frac{\partial F^*_j}{\partial x^*_j} + \frac{\partial F^*_{vj}}{\partial x^*_j} = 0 \tag{1}$$

where superscript '*' represents dimensional variables and

$$U^* = \{\rho^*, \rho^* u_1^*, \rho^* u_2^*, \rho^* u_3^*, e^*\} \tag{2}$$

$$e^* = \rho^*(C_v^* T^* + \frac{1}{2} u_k^* u_k^*) \tag{3}$$

The flux vectors are

$$F^*_j = \left\{ \begin{array}{c} \rho^* u_j^* \\ \rho^* u_1^* u_j^* + p^* \delta_{1j} \\ \rho^* u_2^* u_j^* + p^* \delta_{2j} \\ \rho^* u_3^* u_j^* + p^* \delta_{3j} \\ (e^* + p^*) u_j^* \end{array} \right\} \tag{4}$$

$$F^*_{vj} = \left\{ \begin{array}{c} 0 \\ \tau_{1j}^* \\ \tau_{2j}^* \\ \tau_{3j}^* \\ \tau_{jk}^* u_k^* - q_j^* \end{array} \right\} \tag{5}$$

$$\tag{6}$$

2

where

$$\tau_{ij}^* = -\mu^* \left(\frac{\partial u_i^*}{\partial x_j^*} + \frac{\partial u_j^*}{\partial x_i^*} \right) + 2\mu^*/3 \frac{\partial u_k^*}{\partial x_k^*} \delta_{ij} \quad (7)$$

$$q_j^* = -\kappa^* \frac{\partial T^*}{\partial x_j^*} \quad (8)$$

μ^* is the viscousity coefficient and calculated using the Sutherland's law:

$$\mu^* = \mu_r^* \left(\frac{T^*}{T_0^*} \right)^{3/2} \frac{T_r^* + T_s^*}{T^* + T_s^*}, \quad (9)$$

and κ^* is the heat conductivity coefficient computed by assuming a constant Prandtl number Pr. The gas is assumed to be thermally and calorically perfect gas,

$$p^* = \rho^* R^* T^* \quad (10)$$

where R^* is the gas constant.

3 RESULTS

3.1 Parametric studies on Görtler and shear mode at hypersonic limit

Both shear and Görtler modes at hypersonic speed have been considered in the analysis. Unstable shear mode as well as Görtler mode exist along the concave surface when Reynold's number is large enough; therefore, it is important to investigate which mode is dominant. At hypersonic speed limit, second shear mode dominates the first mode; therefore Görtler modes and second shear modes are compared in the analysis.

Figure 1 shows the maximum temporal growth rates of Görtler and the second shear modes at constant Reynold's number (Re_δ). Each lines of Görtler modes indicates constant Görtler number (G). Reynold's number (Re_δ) is fixed as 1500, and radius of curvature changes in order to study Görtler number effects. As Görtler number increases, the maximum growth rates increase. Increasing Görtler number at fixed Reynolds number represents increase of curvature effects. As curvature increases, flow become more unstable. It is also true for shear mode, but it does not affect the stability condition as much as for Görtler mode. Therefore in figure 1, second shear mode at $G = 15.0$ is only shown.

The figure shows that there is a critical Görtler number above which Görtler mode dominates second shear mode at hypersonic speed limit.

At low Mach number, Görtler modes dominate second shear mode. However, this is the region dominated by first shear modes which are not computed in this analysis. According to Mack's [30] results for flat plate at Re_δ=1500, we can roughly compare growth rates of Görtler modes and first shear modes. If Görtler number is greater than 15.0, Görtler modes dominate first shear modes.

Compressibility effects of Görtler modes are also shown in figure 1. As Mach number increases, growth rate decreases. However, at hypersonic limit, stability effects of compressibility become less important. When Mach number is greater than 5, growth rates become constant. It is the same results as Spall and Malik [10].

3.2 Simulation of flow along the blunt body with concave surface

3.2.1 2-D mean flow

The steady flow solutions of the Navier-Stokes equations for the viscous hypersonic flow over blunt body is simulated using a fifth order explicit upwind scheme and shock fitting method [31]. The test results of the new fifth-order shock fitting scheme and the numerical accuracy of calculating the receptivity problems of hypersonic viscous flows are presented in Ref. [31]. Nine computational zones are used which are resolved by 1449 × 121 grids. Stretched grids are used in streamwise direction as well as in wall normal direction in order to resolve rapid changes of flow properties near the stagnation point in zone 1 and viscous layers. Parameters for the zones are represented in Table 1. Reynold's number is calculated using the flow properties behind the shock, and x-distance from blunt nose to inlet of zone 7 is used as the reference length since disturbances are introduced at the inlet of zone 7 in the simulations of Görtler instability.

First three zones are parabolic blunt body, and concave surface is extended in the other zones. Using polynomial equations, we make continuous and smooth curves. At transition points between two polynomial equations, zeroth, first, and second order derivatives are matched; therefore, curves are continuous till second order derivatives. More smooth curves can be generated by matching the third order and more, but in our analysis, we matched till second order in order to get continuous radius curvature which is a function of

3

Table 1: Parameters for computational zones. Forcing disturbances of the primary Görtler mode are imposed at inlet of zone 7 in simulation.

Zone	X_0	X_l	Re_{X_0}	Re_{X_l}
1	0.00	0.05	0.0	9.39×10^3
2	0.03	0.20	5.43×10^3	6.04×10^4
3	0.18	0.31	4.99×10^4	1.02×10^5
4	0.29	0.51	9.26×10^4	1.91×10^5
5	0.46	0.82	1.67×10^5	3.37×10^5
6	0.74	1.08	2.95×10^5	4.64×10^5
7	1.00	1.34	4.23×10^5	5.92×10^5
8	1.26	1.85	5.52×10^5	8.49×10^5
9	1.71	2.37	7.80×10^5	1.10×10^6

first and second order derivatives. For the concave surface, we used large radius of curvature to avoid shock formation due to the compressive waves inside the computational domains.

The specific flow conditions in free stream are

$$M_\infty = 15$$
$$T_\infty^* = 101.059K$$
$$P_\infty^* = 10.3Pa \qquad (11)$$
$$T_w^* = 1000K$$
$$Re_\infty = \rho_\infty^* U_\infty^*/\mu_\infty^* = 150753.175$$

The body surface is assumed to be a non-slip wall with an isothermal wall temperature T_w^*. Numerical solutions of the steady mean flow are represented in Whang and Zhong [32]. The bow shock shape is obtained as the freestream grid line. The numerical solution for the dimensionless bow shock normal velocities are in order of 10^{-8} - 10^{-9}.

3.2.2 Inlet disturbances obtained from LST

Inlet forcing disturbances are obtained by linear stability analysis using simulated 2-D mean flow. Concave surfaces are included in zone 4 and beyond. Calculated Görtler number is between 2.5-13.0, and Mach number behind shock is 6-9.1. Mach number and Görtler number distributions along streamwise direction for zone 5 - 9 are shown in figure 2. Since Görtler number is relatively low at such high Mach number, zone 4 and 5 do not have unstable modes in LST calculation. At the end of zone 6, we found unstable Görtler mode, therefore, the forcing disturbances are introduced at inlet of zone 7. Eigenfunctions of the primary modes obtained from linear stability analysis are

shown in figure 3. Flow properties are nondimensionalized by freestream values such as streamwise velocities by U_∞^*, normal and spanwise velocities by $U_\infty^*/\sqrt{Re}$, pressure by $\rho_\infty^* U_\infty^{*2}/Re$, length scales by x_0^* of zone 7 in the streamwise direction, and by boundary layer thickness,δ in normal and spanwise directions, and time scale by x^*/U_∞^*. Nondimensional spanwise wavenumber, β, is 0.1. The growth rate (σ_i) of primary mode is 1.014. Figure 4 shows streamwise velocity perturbation contour of primary Görtler mpde. The growth of Görtler vortices in the streamwise direction is shown by intensity of the disturbances. The figure also shows the distributions of the simulated disturbances in wall normal direction at $I = 100$. LST results are also plotted in the same figure. u_r and T_r from DNS are matched will with those from LST. More detailed linear growth of the primary and secondary Görlter modes were investigated in Whang and Zhong [32].

3.3 Non-linear Growth of Görtler Vortices

It is an important topic how Görtler vortrices break down to turbulence. Experiments showed that it is mainly due to the interaction of nonlinear growth of Görtler vortices and other forms of disturbances. In nonlinear growing process, mushroom shaped vortices are produced since the counter-rotating vortices pump fluid with a low streamwise velocity away from the wall. There are two regions in Görtler vortices which are peak (low velocity region) and valley (high velocity region). These two regions produce the mushroom shaped vortices. Interaction between these vortices and traveling wave is the main factor of breaking down to turbulence.

To study nonlinear effects of Görtler instability, large amplitude disturbances are introduced at inlet of zone 7. The amplitude of the inlet Görtler mode is about $0.1U_\infty$. Five zones (zone 7, zone 8, zone 9, zone 10 and zone 11) are used in nonlinear simulation. Two more zones are extended for nonlinear calculations. Each zones are resolved by $161 \times 121 \times 64$ grids. In the simulation, parallel computing is applied to reduce the computational time. Six nodes are applied to each zones.

Figure 5 and figure 6 show streamwise mean velocity distributions as flow moves downstream. The development of mushroom shaped vortices is well represented in the figure. Bow shock does not have much effects on flow field since Görtler vortices develop in viscous layers. The iso-contours of streamwise mean velocity at four different streamwise locations are shown in figure 7. Peak and valley regions are clearly shown. While

the middle region (peak) tends to go up, others becomes narrower.

Profiles of the streamwise velocity in wall normal direction at four different spanwise locations are shown in figure 8. Velocity in peak region increases near the wall, and inflection points develop. The Görtler vortices pump vertically the low-speed fluid away from the wall in the peak region and push the high speed fluid toward the wall in the valley region. However, there is the limitation of growing thickness of the peak, and high speed fluid starts to transfer to the peak region near the wall and the low speed fluid to the valley away from the wall. As a results, the mushroom shaped vortices are produced. Streamwise velocity perturbation contours shown in figure 9 represent fluid near the wall in peak region is transferred to the valley.

In Görtler instability, inflection points develop in wall normal and spanwise directions, and inviscid instability problem becomes important which induces the secondary instability. Derivatives of the streamwise velocity show clear development of inflection points. Figure 10 shows iso-contour of $\rho \frac{\partial U}{\partial y}$ in four different streamwise locations. Structure in peak region (low velocity region) changes as flow moves. The vertical shear has its maximum in the low velocity region. Wall normal distributions of the normal streamwise velocity gradients are shown in figure 11 in which the magnitude of $\rho \frac{\partial U}{\partial y}$ is the maximum. Inflection points develop in the peak region. At $X = 1.042$, there is no inflection points; however, as the flow moves to downstream, they develop and the magnitude increases which means that effects of inflection points increase.

The same trends are observed in spanwise velocity gradients. Figure 12 and 13 show profiles of spanwise velocity gradients, $\rho \frac{\partial U}{\partial z}$, at four different streamwise locations. Both figures also represent the development of inflection points. Inflectional profiles appear in spanwise direction as well as normal direction, and they are related to the secondary instability. Using energy conversion mechanism, Yu and Liu[21] showed that sinuous mode of secondary instability is related to normal velocity gradient, and varicos mode is related to the spanwise gradient.

Figure 14 shows streamwise vorticity contours. Counter rotating streamwise vortices are well represented in this figure. The structure of the velocity field is shown in figure 15 as the cross sectional vector plot in four different streamwise directions. It also shows that the counter rotating streamwise vortices and pumping action with low velocity away from the wall. This effect become stronger in downstream. In addition, as flow moves, structure becomes complex due to nonlin-

ear effects, and it will break down to turbulent. The complexity is also shown in figure 10 and figure 12. Nonlinear breakdown of Görtler vortices will be investigated by extending more zones.

There are two peaks in iso-contours of spanwise velocity gradients, and flow properties changes. Therefore, X-Z cross sections are plotted for various flow parameters. Figure 16 is the cross sectional plots for streamwise velocity. From figure 9, high velocity disturbances near the wall moves toward the peak region, and the low velocity away from the wall moves to the valley. Therefore near the wall ($J = 42$), minimum velocity region become narrower However, low velocity disturbances away from the wall transferred from the valley goes down since counter rotating vortices pushes down the flow at the valley region. That's why there are two minimum peak regions near the center ($J = 69$) as flow moves downstream. Spanwise velocity gradient (figure 17) and streamwise vorticity (figure 18) profiles also represent the effects of counter rotating vorticity. Near the wall the peak region moves toward the center, but opposite trends occurs away from the wall. Both figures also show that flow becomes complicated downstream.

Finally, we studied spanwise Fourier spectral modes on nonlinear growth of Görtler vortices. The number of spanwise Fourier modes used in the z-direction is 33. The energy in each Fourier mode is shown in figure 19. Energy is defined as

$$E_n = \int_0^\infty (|u_n|^2 + |v_n|^2 + |w_n|^2)dy. \tag{12}$$

Initially, the Görtler vortex (mode 1) develops linearly. Mean flow correction mode (mode 0) dominates mode 1 as the flow moves downstream. In this nonlinear regime, the main interaction is between the fundamental and mean flow correction mode (mode 0). However, effects of higher modes (mode 2, 3, etc) increase as flow moves downstream. Those modes will increase and be saturated. If the flow reaches this condition, it will break down to turbulence.

Figure 20 and figure 21 show the eigenfunction comparison between simulated results and those obtained from local LST. Simulated results near the inlet of zone 7 are well matched with LST. It means that disturbances grow linearly at the beginning. However, after higher mode and mean flow correction mode effects become significant, the results are not compatible since nonlinear effects are significant.

In figure 22 and figure 23, mode shapes for streamwise velocity and temperature at four different stream-

5

wise locations are plotted. Hall [17] in his incompressible Görtler instability analysis shows that shape of U_1 changes significantly compared to linear solution as flow moves downstream. However, in our hypersonic Görtler analysis, the shape of second mode for streamwise velocity and temperature changes more dramatically than the fundamental mode. It is a difference between incompressible analysis and our compressible analysis. In our analysis, the disturbance is dominated by the fundamental and mean flow correction which is also true for Hall's [17]. However, magnitude of the second mode is the almost same order of the fundamental and mean flow correction modes.

3.4 Nonlinear interaction of Görtler and second shear mode

Experiments showed that Görtler vortices break down to turbulence due to secondary instability. Nonlinear development of Görtler vortices produce comlicated structure which will break down. However, interaction of Görtler vortices with other form of disturbances leads earlier transition to turbulence.

3.4.1 Simulation of second shear mode without Görtler vortices

First we imposed the second shear mode at inlet of zone 7 and compared the simulated results with those obtained from LST in order to verify the simulation code. 2-D mean flow without Görtler vortices is used in this analysis. Inlet disturbances which are shown in figure 24 are obtained from LST. Profile of pressure disturbance (p_r) represents that it is second shear mode. At hypersonic speed limit, second mode dominates first mode; therefore, we found the second. However, in our linear stability analysis, there is no unstablle shear mode, and we choose one stable mode and impose it at inlet of zone7 in the analysis with and without Görtler vortices.

Spatial stability analysis is considered. In other words, frequency, ω, is real, and wavenumber, α, is complex. In the analysis, the nondimensional frequence is 120. Figure 25 show disturbance contours at certain time after disturbances propagate spatially and reach the periodic condition. The figure shows disturbances decay as the flow moves downstream. Decaying disturbances are more clearly shown in figure 26 which represents disturbance distributions along the streamwise direction at a certain wall normal position.

The simulated results are compared with those pre-

Table 2: Growth rates obtained from DNS at three different locations are compared with those from LST. Positive sign of the growth rate represents the mode is stable.

X	$\alpha_i(LST)$	$\alpha_i(DNS)$	$error(\%)$
1.043866	5.84966	6.20078	6.0
1.056898	5.95504	6.32484	6.2
1.086860	6.19107	6.67196	7.8

dicted by LST. Figure 27 shows the disturbance distributions at $X = 1.056898$ ($X = 1.0$ is at inlet of zone 7). There is a good agreement between DNS and LST. Growth rate (α_i) and phase (α_r) are also compared. Growth rates at three different streamwise locations are shown in table 2. Growth rate for DNS is computed using:

$$\alpha_i = \frac{1}{|\phi|} \frac{d|\phi|}{dX} \qquad (13)$$

where ϕ is the amplitude of disturbances and is compared one from LST. The error is around 6 to 7 %. α_r for simulation is computed using

$$\alpha_r = \frac{2\pi}{\lambda} \qquad (14)$$

where λ is the wavelength. Phase angle is plotted in figure 28. From the figure, the wavelength is calculated which is 0.04581, and it leads α_r is 137.15739. α_r from LST is 133.746 which agrees well with one from DNS. Fourier transformation is used in order to compute amplitude and phase angle of disturbances.

3.4.2 Effects of Görtler vortices on second shear mode

Nonlinear interaction of second shear mode and Görtler mode is considered. The second mode is imposed at inlet of zone 7 in which steady Görtler mode exists. The amplitude of the shear mode is 1% of the freestream velocity which is one order lower than imposed Görtler mode. Nondimensional frequency and inlet disturbances of the shear mode are the same as those in previous section.

Figure 29 and Figure 31 show the cross sectional distributions of the shear mode in the existence of Görtler mode. Figure 29 is for the region near the surface, and

6

figure 31 is for inflectional region. Both figures show the development of complex structure as the flow moves downstream due to the nonlinear interaction between shear and Görtler mode. We imposed 2-D TS waves at the inlet of zone 7, but oblique mode develops along the streamwise direction. Disturbances imposed in the middle propages slower than those at side which represents the development of oblique mode.

The imposed shear mode is stable according to linear stability analysis. DNS results show that the mode is stable in the existence of Görtler mode except near inflectional region. Figure 30 show distributions of temperature disturbances near the surface along streamwise direction at three different spanwise locations. Decaying disturbances are well represented in the figure. However, in figure 32, disturbances are excited as the flow moves downstream due to the nonlinear interaction. Nonlinear development of Görtler vortices produce inflectional profiles which destabilize the shear mode. Figure 8 shows that inflectional profiles start to develop at valley region $(K = 4)$. Inflection points at peak region appear later station. However, in zone 7, there is no inflection points near the peak region. Therefore, disturbances imposed near the valley region increase along the streamwise direction $(Z = 0.0$ and $Z = 0.11$ in figure 32). However, those in which there is no inflection points decay. This trend is well represented in streamwise velocity profile in figure 33.

4 CONCLUSIONS

In this paper, nonlinear development of Görtler vortices and its interaction with second shear mode were investigated. Parametric studies on relation between Görtler and shear modes were considered by linear stability analysis. At hypersonic speed limit, the maximum growth rates of Görtler and shear modes were computed. Mach number varied 1 to 8, and Re_δ is fixed as 1500. There is a critical Görtler number over which Görtler modes are dominant. Increase of Görtler number indicates increase of concave surface effects. Concavity destabilizes the flow, but it affects more Görtler modes than shear mode. Changing curvature causes dramatic changes in growth rate of Görtler mode but little changes for the second shear mode.

Mean flow along the blunt body which includes concave wall was simulated by a fifth-order explicit unsteady computer code. Disturbances for Görtler and second shear mode were computed using the stability code and added in inlet of zone 7. Simulation results were compared with results predicted by LST. There were good agreements between two results.

We studied nonlinear effects of Görtler vortices. Simulation showed the development of high and low velocity regions in Görtler vortices. The transfer of high speed fluid in valley region into the peak produced mushroom shaped vortices. Inflection points developed in nonlinear growth of Görtler vortices. The profiles of normal and spanwise velocity gradient showed the inflectional points which induce the inviscid instability problem.

Finally, nonlinear interaction of Görtler and second shear mode was considered. Due to development of inflection points in nonlinear effects of steady Görtler mode, stable 2-D shear mode was excited, and oblique mode was developed as the flow moves downstream.

5 Future Works

Work is in progress to include more detailed nonlinear interaction between Görtler mode and other forms of disturbances. Secondary instability of Görtler vortices at hypersonic speed will be investigated using DNS and Floquet theory. Fundamental and subharmonic secondary instability will be considered. Mixing effects in the existence of fuel injection will also be studied. There are concave surfaces at engine inlet of hypersonic vehicle in which Görtler vortices and fuel injection exist.

6 ACKNOWLEDGEMENTS

References

[1] Görtler, H., "Instabilita-umt laminarer Grenzchichten an Konkaven Wäden gegenber gewissen dreidimensionalen Störungen," *ZAMM*, Vol. 21, 1941, pp. 250–52.

[2] Liepmann, H. W., "Investigation of boundary layer transition on cancave walls," *NACA Rep.*, Vol. W-107, 1945.

[3] Tani, I., "Production of longitudinal vortices in the boundary layer along a concave wall," *J. Geophysical Res.*, Vol. 67 no 8, 1962, pp. 3075–3080.

[4] Smith, A., "On the growth of Taylor-Görtler vortices along highly concave wall," *Quart. J. Math.*, Vol. 13, 1955, pp. 233–262.

[5] Hall, P., "Taylor-Görtler vortices in fully developed or boundary-layer flows: linear theory," *J. Fluid Mech.*, Vol. 124, 1982, pp. 475–494.

[6] Hall, P., "On the non-linear evolution of Görtler vortices in non-parallel boundary layers," *IMA J. Appl. Math.*, Vol. 29, 1982, pp. 173–196.

[7] Hall, P., "The linear development of Görtler vortices in growing boundary layers," *J. Fluid Mech.*, Vol. 130, 1983, pp. 41–58.

[8] Hall, P. and Fu, Y., "On the Görtler vortex instability mechanism at hypersonic speed," *Theoret. Comput Fluid Dynamics*, Vol. 1, 1989, pp. 125–34.

[9] El-Hady, N. M. and Verma, A. K., "Growth of Görtler vortices in compressible boundary layers along curved surfaces," *J. Engineering and Appl. Sciences*, Vol. 2, 1983, pp. 213–38.

[10] Spall, R. E. and Malik, M. R., "Görtler vortices in supersonic and hypersonic boundary layers," *Phys. Fluids*, Vol. 1(11), 1989, pp. 1822–35.

[11] Aihara, Y., "Görtler vortices in the nonlinear region," In Theoretical and Experimental Fluid Mechanics, ed U. Müller, K. G. Roesner, B. Schmidt, pp 331-38. Berlin:Springer-Verlag, 1979.

[12] Sabzvari, J. and Crane, R. I., "Effect of Görtler vortices on transitional boundary layers," *ASME FED*, Vol. 32, 1985.

[13] Peerhossaini, H. and Wesfreid, J. E., "Experimental study of the Taylor-Görtler Instability," In Propagation in Systems Far From Equilibrium, ed. J. E. Wesfreid, H.R. Brand, D. Manneville, G. Albinet, N. Boccara, et al, pp. 399-412. Berlin:Springer-Verlag, 1988.

[14] Aihara, Y. and Koyama, H., "Nonlinear development and secondary instability of Görtler Vortice," In Stability in the Mechanics on Continua, ed F. H. Schroeder, pp 345-54. Berlin: Springer-Verlag, 1982.

[15] Aihara, Y., Tomita, Y., and Ito, A., "Generation, development and distortion of longitudinal vortices in boundary layers along concave and flat plates," In Laminar-Turbulent Transition, ed V. V. Kozlov, pp. 447-54. New York:Springer-Verlag, 1985.

[16] Swearingen, J. D. and Blackwelder, R. F., "The growth and breakdown of streamwise vortices in the presence of a wall," *J. Fluid Mech.*, Vol. 182, 1987, pp. 255–290.

[17] Hall, P., "The nonlinear development of Görtler vortices in growing boundary layers," *J. Fluid Mech.*, Vol. 193, 1988, pp. 243–66.

[18] Lee, K. and Liu, T. C., "On the growth of mushroomlike structure in nonlinear spatially developing Görtler vortex flow," *Phys. Fluids A*, Vol. 4(1), 1992, pp. 95–103.

[19] Liu, T. C., "On scalar transport in nonlinearly developing Görtler vortex flow," *Geophys. Astrophys. Fluid Dynamics*, Vol. 58, 1991, pp. 133–45.

[20] Liu, W. and Domaradzki, J. A., "Direct numerical simulation of transition to turbulence in Görtler flow," *J. Fluid Mech.*, Vol. 246, 1993, pp. 267–299.

[21] Yu, X. and Liu, T. C., "On the mechanism of sinous and varicose modes in three-dimensional viscous secondary instability of nonlinear Görtler rolls," *Phys. Fluids*, Vol. 6(2), 1994, pp. 736–50.

[22] Li, F. and Malik, M., "Fundamental and subharmonic secondary instabilities of Görtler vortic es," *J. Fluid Mech.*, Vol. 297, 1995, pp. 77–100.

[23] Nayfeh, A. H., "Effect of streamwise vortices on Tollmien-Schlichting waves," *J. Fluid Mech.*, Vol. 107, 1981, pp. 441–453.

[24] Malik, M. R., "Wave interaction in three dimensional boundary layers," *AIAA Paper 86-1129.*, 1986.

[25] Nayfeh, A. H. and Al-Maaitah, A., "Influence of streamwise vortices on Tollmien-Schlichting waves," *Phys. Fluids*, Vol. 31(12), 1988, pp. 3543–3549.

[26] Malik, M. R. and Hussaini, M. Y., "Numerical simulation of interaction between Görtler vortices and Tollmien-Schlichting waves," *J. Fluid Mech.*, Vol. 210, 1990, pp. 183–199.

[27] Hall, P., "Görtler vortices in growing boundary layers: the leading edge receptivity problem, linear growth and the nonlinear breakdown stage," *Mathematika*, Vol. 37, 1990, pp. 151–189.

[28] Floryan, J. M., "On the Görtler instability of boundary layers," *Prog. Aerospace Sci.*, Vol. 28, 1991, pp. 235–271.

[29] Saric, W. S., "Görtler vortices," *Annual Review of Fluid Mechanics*, 1994, pp. 379–409.

[30] Mack, L. M., "Boundary layer linear stability theory," *AGARD Rep. No. 709*, 1984.

[31] Zhong, X., "Direct numerical simulation of hypersonic boundary-layer transition over blunt leading edges, part I: a new numerical method and validation," *AIAA Paper 97-0755*, 1997.

[32] Whang, C. and Zhong, X., "Direct numerical simulation of Görlter instability in hypersonic boundary layers," *AIAA Paper 99-0291*, 1999.
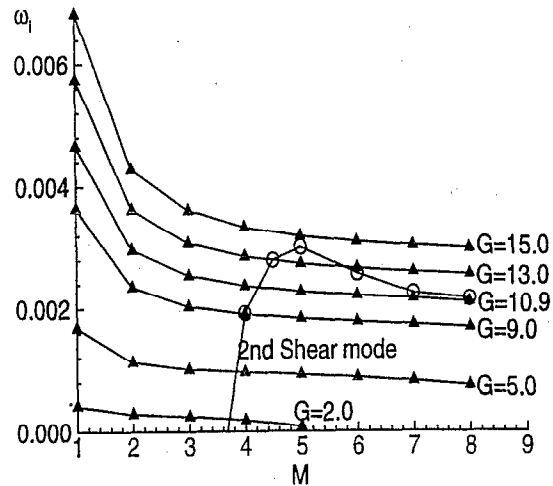
Figure 1: Comparison of the maximum growth rates of Görtler modes and second shear modes at $Re_\delta = 1500$. There is a critical Görtler number above which Görtler modes are dominant.
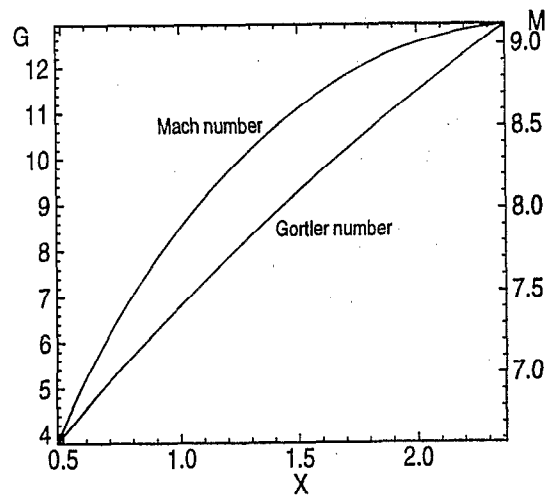
Figure 2: Distributions of Görtler number and Mach number behind shock. Mach number increases because a shock becomes weaker, and Görtler number increases since Reynold's number increases.
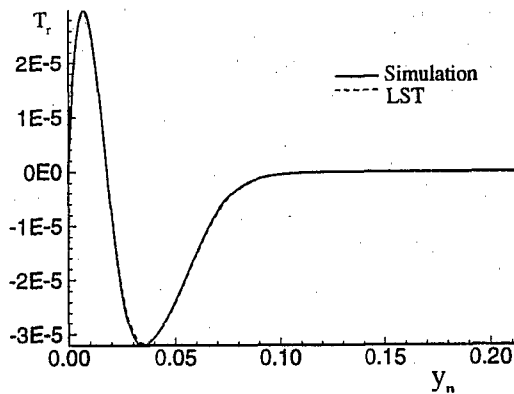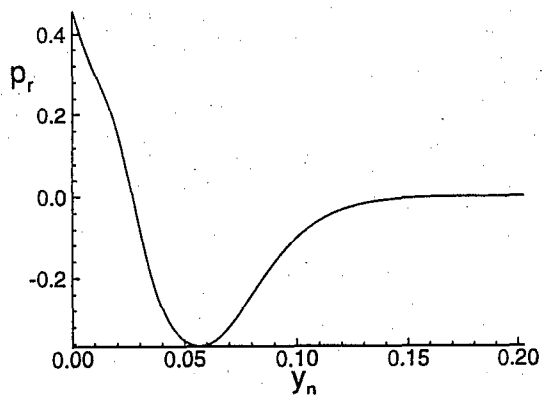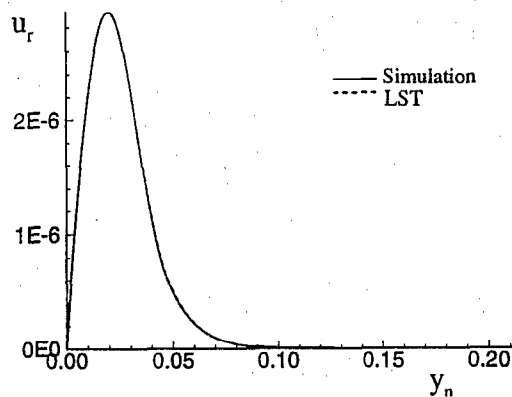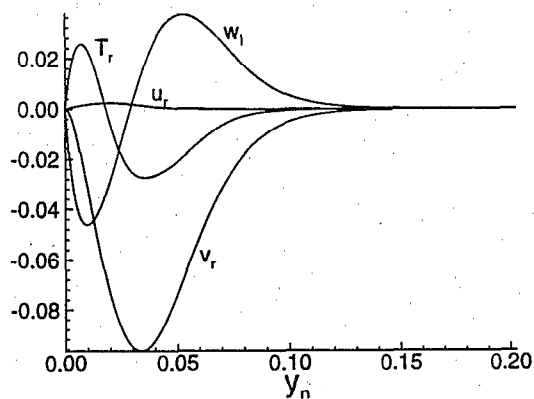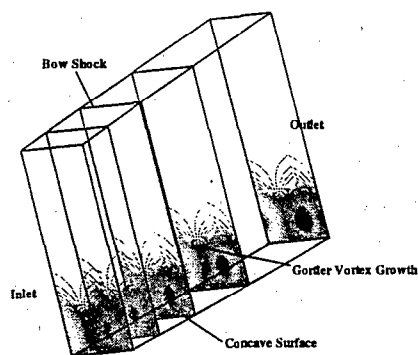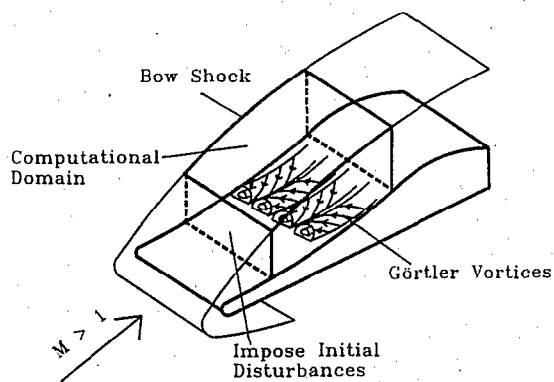
Figure 3: Schematic of computational domain and eigenfunctions of primary Görtler mode of inlet of zone 7 at $G = 6.71$, $M = 7.89$, $Re_x = 4.23 \times 10^5$, and $\beta = 0.1$. Growthrate (σ_i) is 1.014.

Figure 4: Streamwise velocity perturbation contours and wall normal distributions of u_r and T_r at $I = 100$ of zone 7 at $G = 6.71$, $M = 7.89$, $Re_x = 4.23 \times 10^5$, and $\beta = 0.1$. Results are compared with those obtained from LST.

10
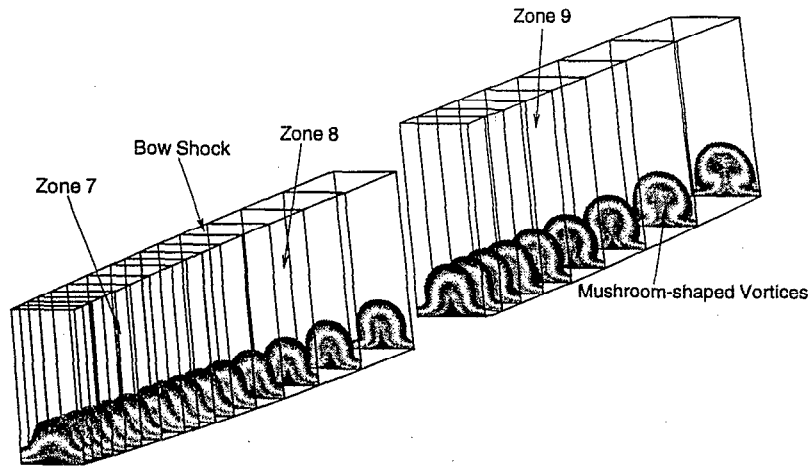
Figure 5: Distributions of iso-contours of streamwise mean velocity along the streamwise direction for zone 7, 8 and 9. The size of grids is $483 \times 121 \times 64$. Mushroom shaped vortices develop as flow moves downstream due to nonlinear effects.
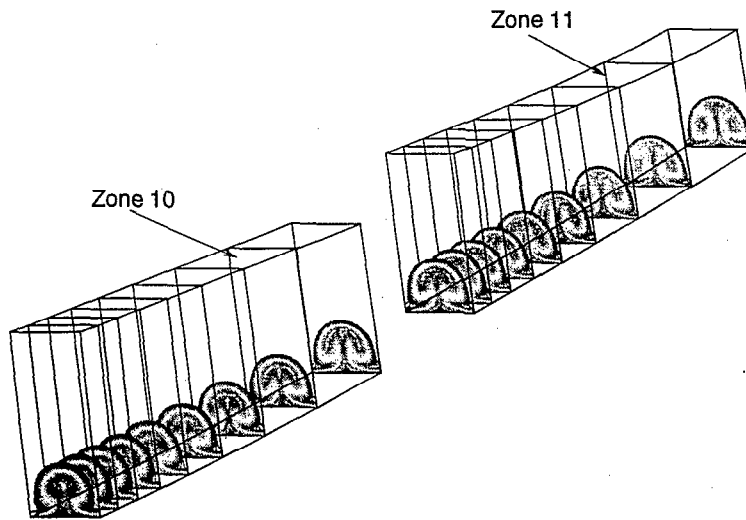
Figure 6: Distributions of iso-contours of streamwise mean velocity along the streamwise direction for zone 10 and 11.

11
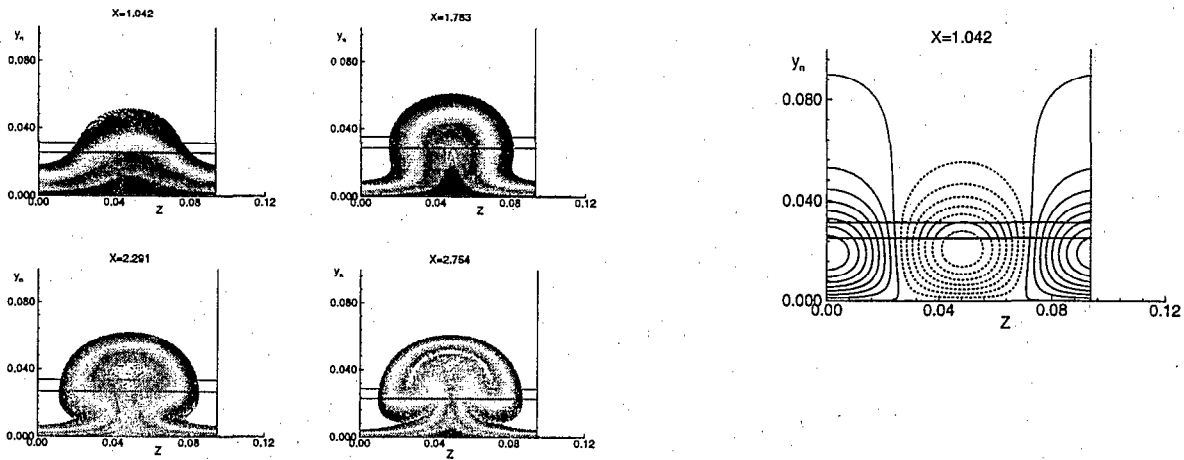
Figure 7: Sectional streamwise velocity distribution at four different streamwise locations.
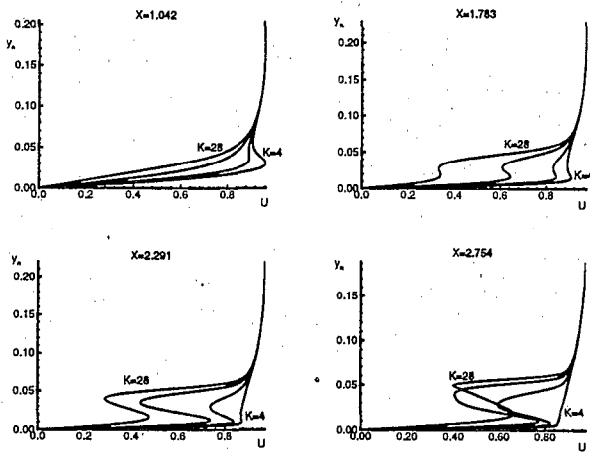
Figure 8: Profiles of the streamwise velocity in wall normal direction at four different streamwise locations. Velocity of the peak region (K=28) near the wall increases as flow moves downstream.
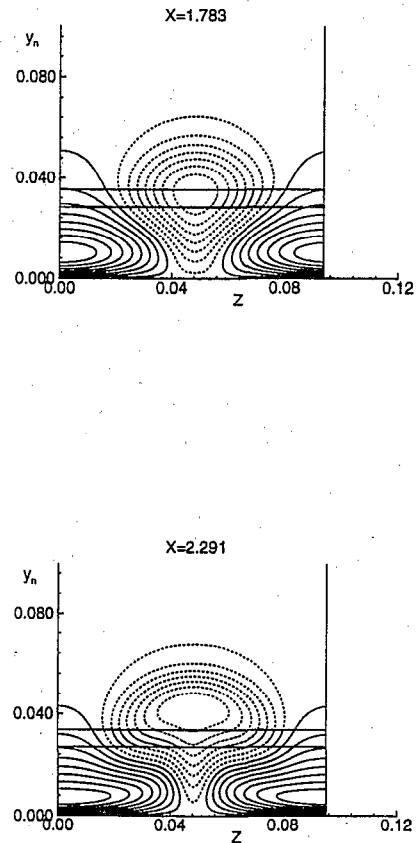
Figure 9: Streamwise velocity disturbance contours at four different streamwise locations. Disturbances in valley region near the wall moves to the peak region of Görtler vortices.
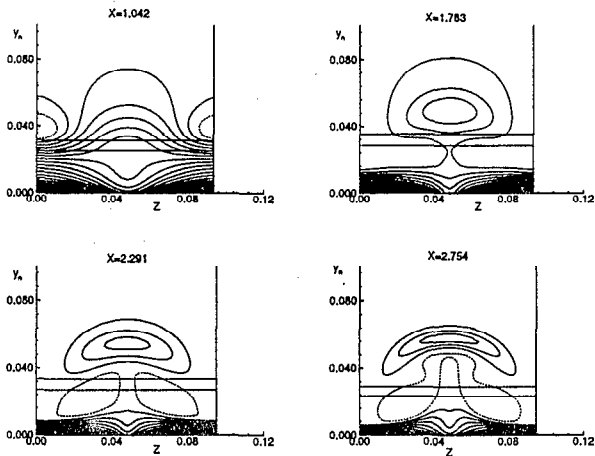
Figure 10: Iso-contours of normal gradient of the mean streamwise velocity in the cross-stream plane at four different streamwise locations.
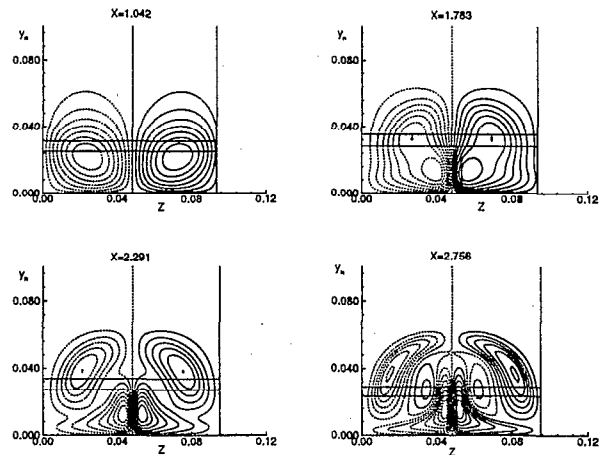
Figure 12: Iso-contours of spanwise gradient of the mean streamwise velocity in the cross-stream plane at four different locations.
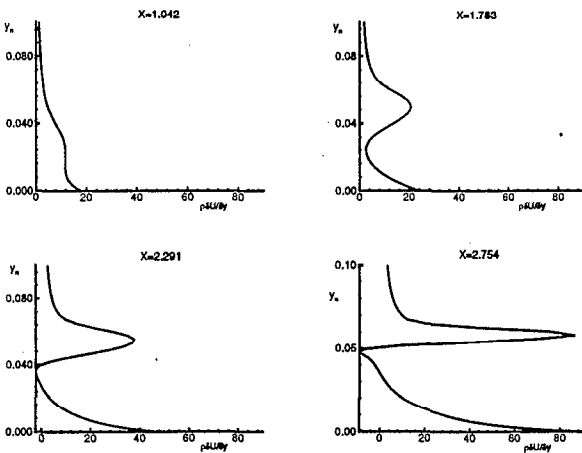
Figure 11: Profiles of normal gradient of the mean streamwise velocity in wall normal direction at peak region. Inflection points develop along the streamwise direction.
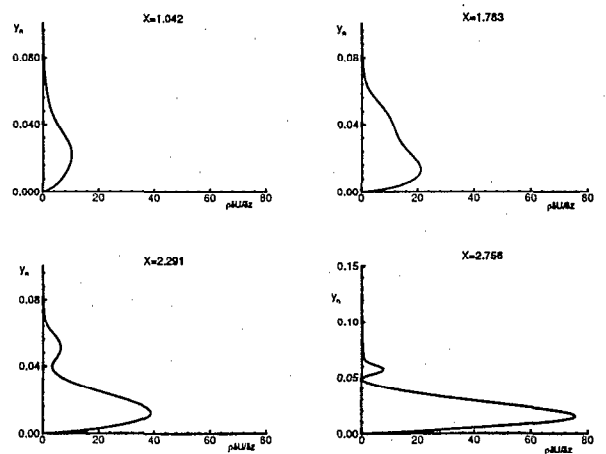
Figure 13: Profiles of spanwise gradient of the mean streamwise velocity in wall normal direction. Inflection points develop along the streamwise direction.
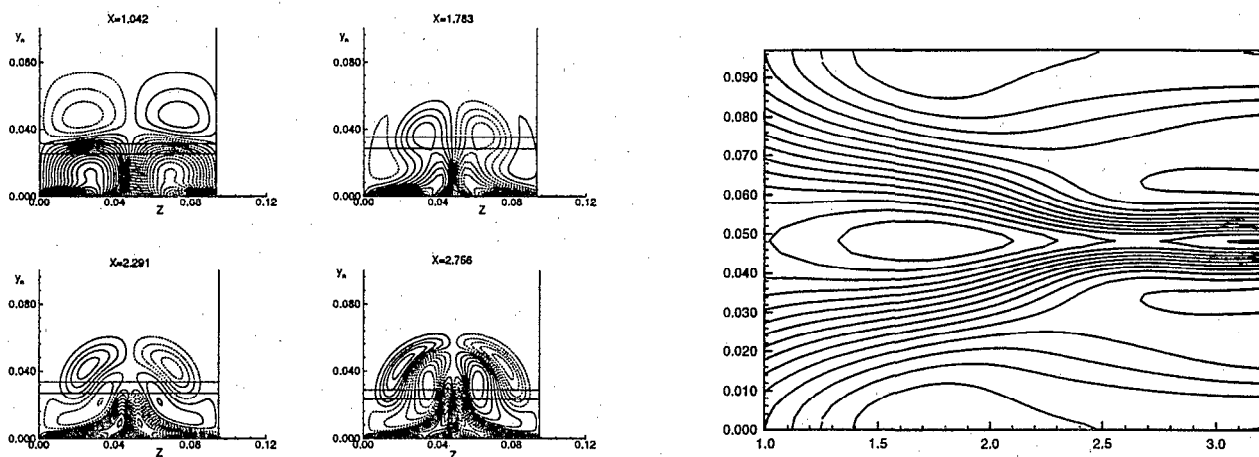
Figure 14: Streamwise vorticity contours at four different streamwise directions. Counter rotating vorticity is well represented.
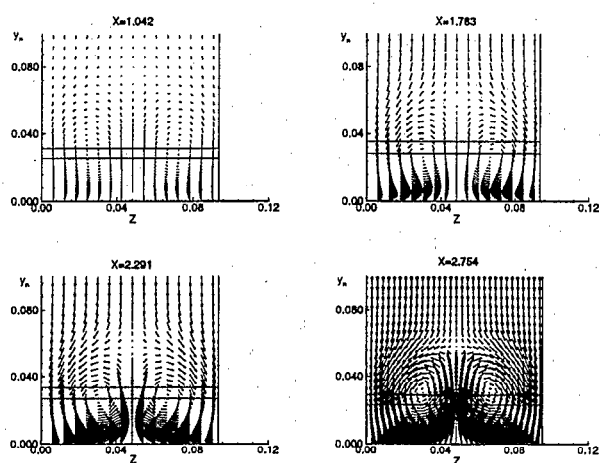
Figure 15: Structure of the velocity vector field in the plane normal to the wall.
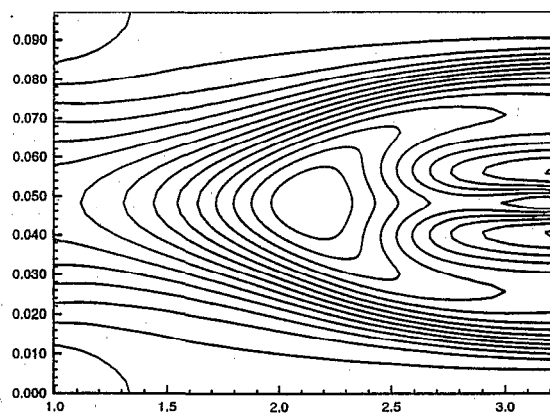
Figure 16: Streamwise mean velocity in the (X,Z)-plane at $J = 42$ (up) and $J = 69$ (bottom)

14
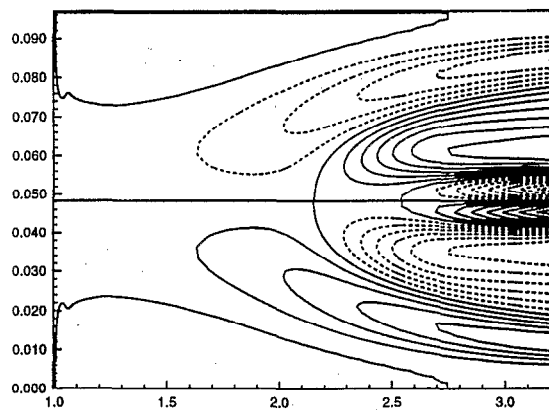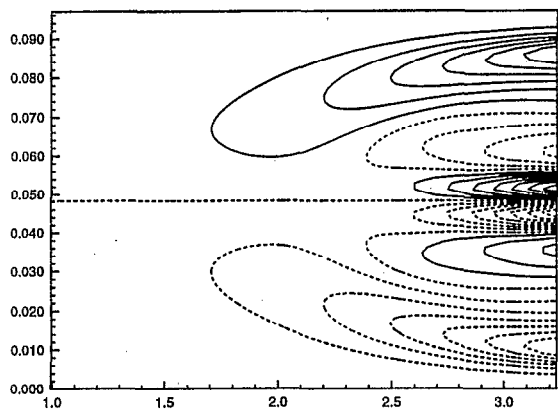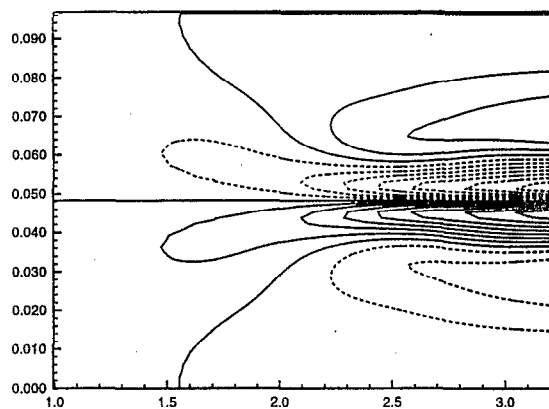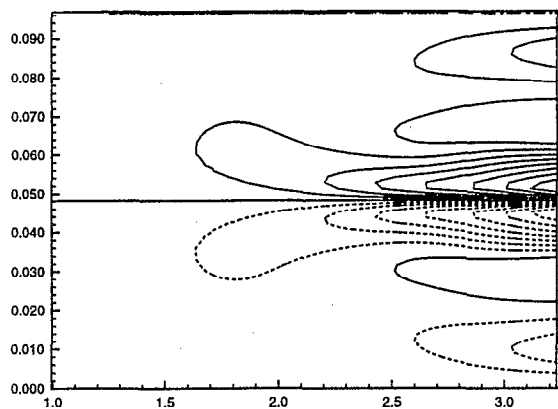
Figure 17: Spanwise velocity gradient profiles in the (X,Z)-plane at $J = 42$ (up) and $J = 69$ (bottom)

Figure 18: Distributions of streamwise vorticity in the (X,Z)-plane at $J = 42$ (up) and $J = 69$ (bottom)

15
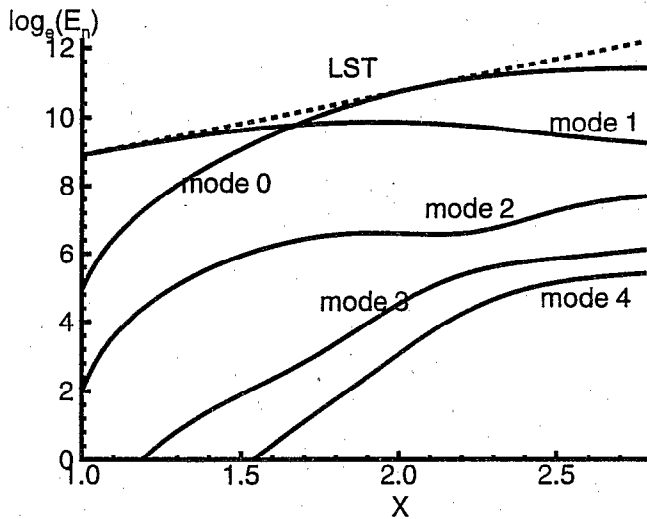
Figure 19: Nonlinear evolution of disturbance energy for various spanwise Fourier modes.
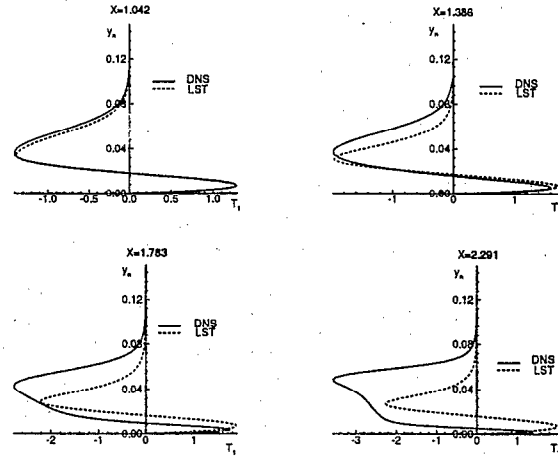
Figure 21: Temperature disturbance comparison between DNS and local LST results. Disturbances grow linearly near the inlet of zone 7.
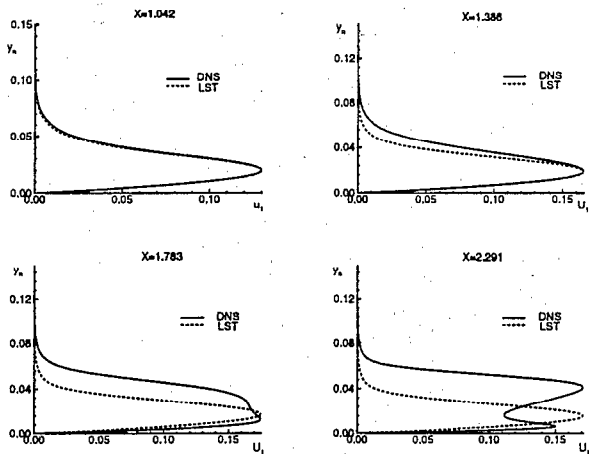
Figure 20: Streamwise velocity disturbance comparison between DNS and local LST results. Disturbances grow linearly near the inlet of zone 7.
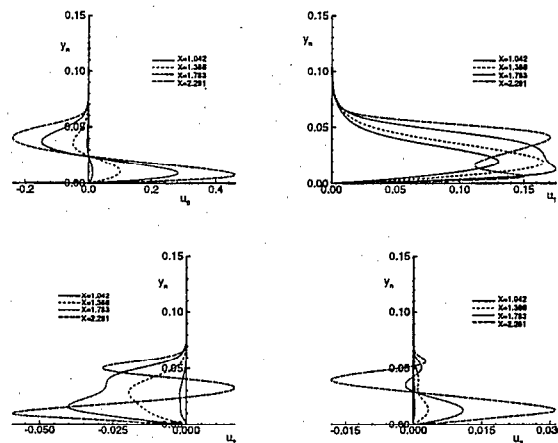
Figure 22: Streamwise velocity profiles for mode 0, 1, 2, and 3 at four different streamwise locations.
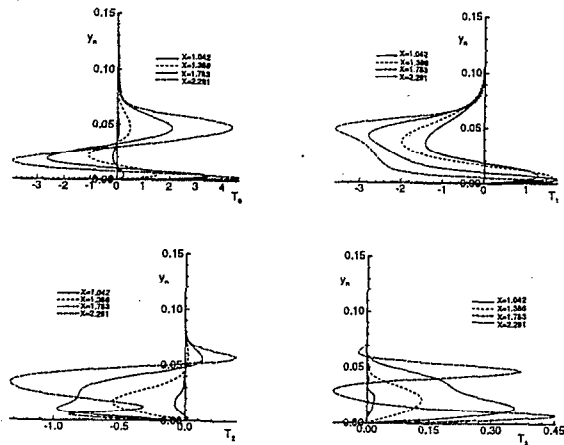
Figure 23: Temperature profiles for mode 0, 1, 2, and 3 at four different streamwise locations.
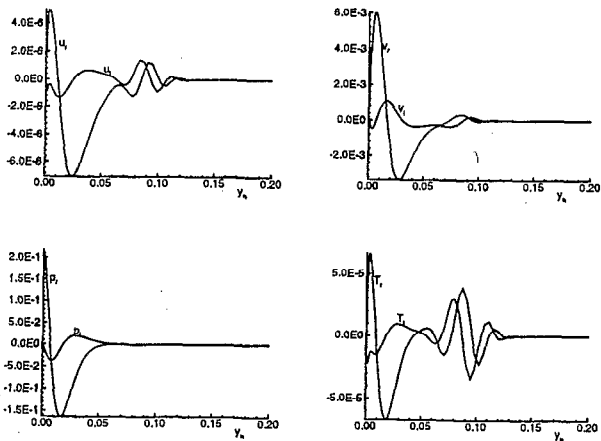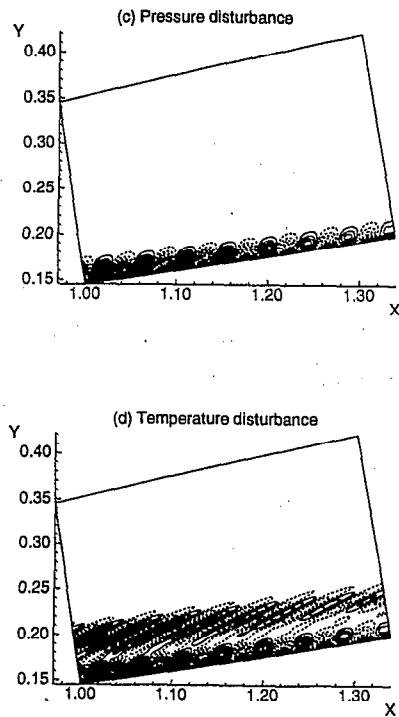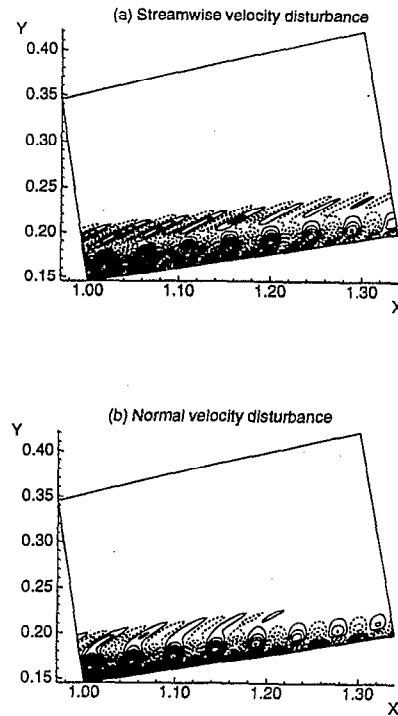
Figure 24: Eigenfunctions of the second shear mode which are imposed inlet of zone7.

Figure 25: Distributions of disturbances without interaction with Görlter modes. Disturbances decay along the streamwise direction.

17
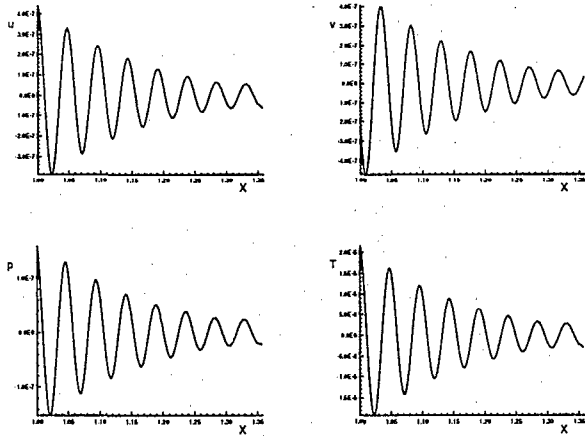
Figure 26: Distributions of disturbances along the streamwise locations show that the mode is stable.
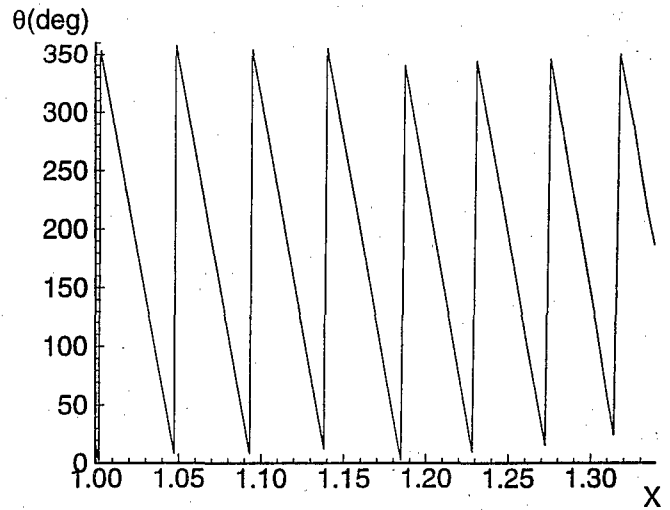
Figure 28: Phase angle of disturbances obtained from Fourier transformation analysis.
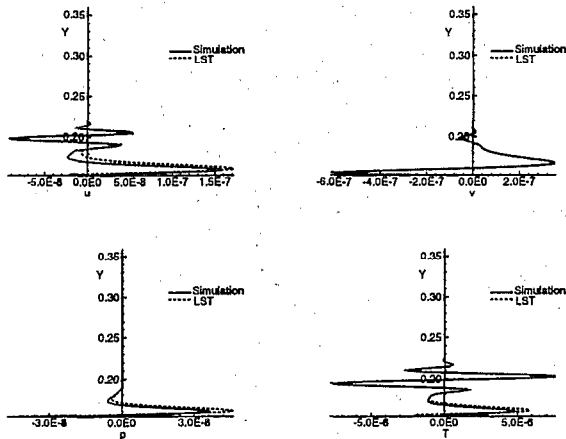
Figure 27: Comparison between simulated results and those obtained from LST (I=50). They give a good agreement
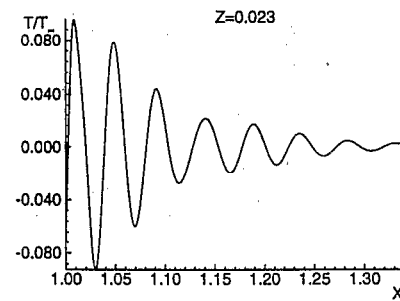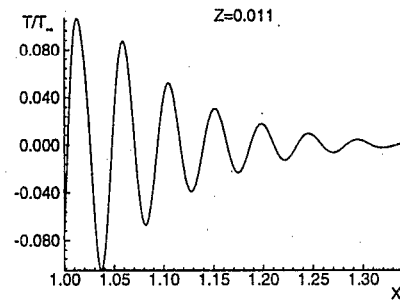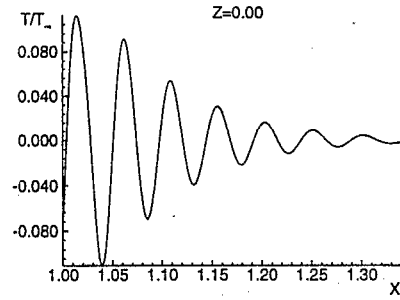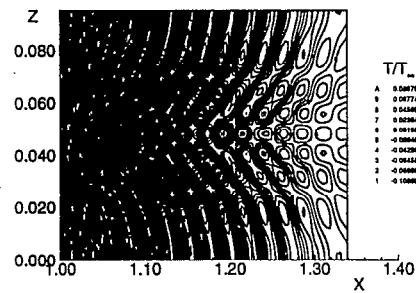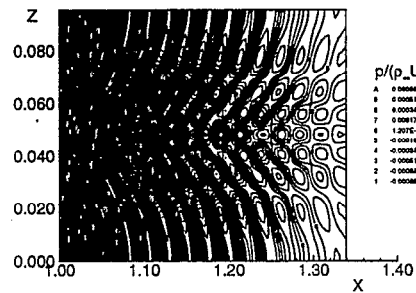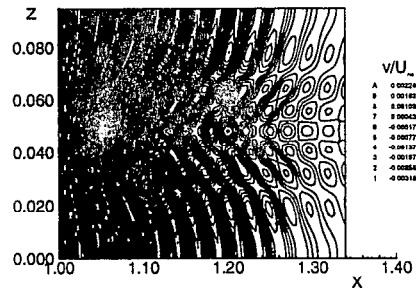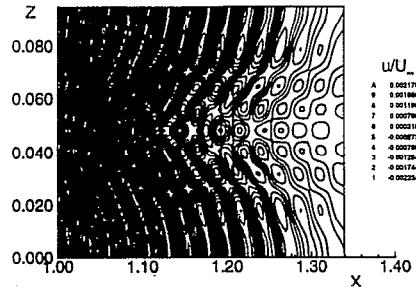
Figure 29: Sectional distributions of shear mode near the surface in the existence of Görtler mode. Complicated structures appear as the flow moves downstream due to the nonlinear interaction.

Figure 30: Imposed shear mode near the surface decay in the existence of Görtler mode.

19
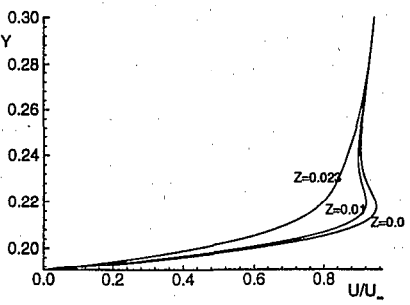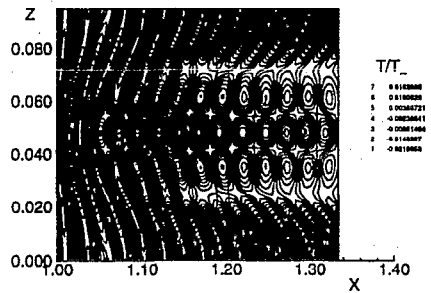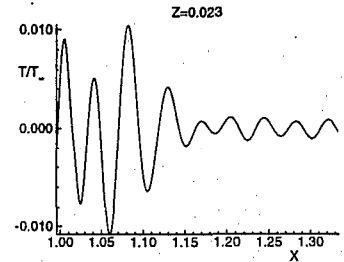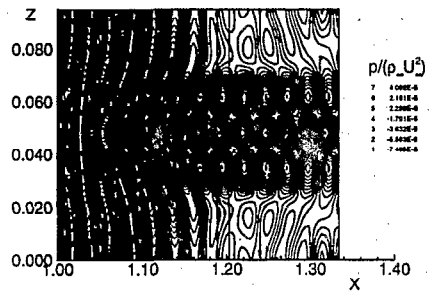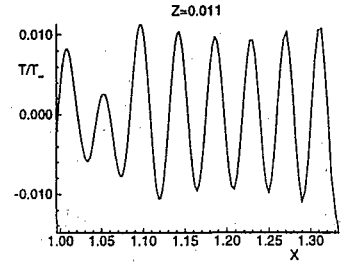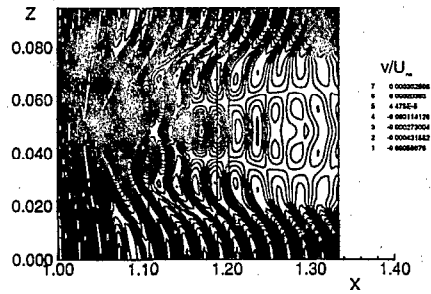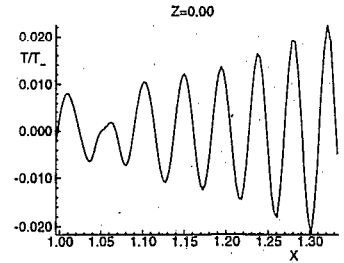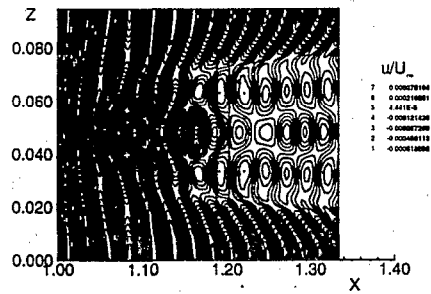
Figure 31: Sectional distributions of shear mode in the existence of Görtler mode in which there is an inflection point. Structure become complicated as the flow moves downstream due to the nonlinear interaction.

Figure 32: Disturbances imposed at inflection region increase as the flow moves down stream.

Figure 33: Inflectional profiles develop along wall normal direction. Disturbances increases in which there is a inflection point.